Magnetically and optically tunable terahertz radiation from Ta/NiFe/Pt spintronic nanolayers generated by femtosecond laser pulses

Roman Adam (iD), Genyu Chen (iD), Daniel E. Bürgler, Tianyu Shou (iD), Ivan Komissarov, Sarah Heidtfeld, Hilde Hardtdegen (iD), Martin Mikulics, Claus M. Schneider (iD), and Roman Sobolewski (iD)

View Online   Export Citation   CrossMark

ARTICLES YOU MAY BE INTERESTED IN

Magnetically and optically tunable terahertz radiation from Ta/NiFe/Pt spintronic nanolayers generated by femtosecond laser pulses

View Online   Export Citation   CrossMark

Roman Adam,[1,a] (iD) Genyu Chen,[2] (iD) Daniel E. Bürgler,[1] Tianyu Shou,[3] (iD) Ivan Komissarov,[3] Sarah Heidtfeld,[1] Hilde Hardtdegen,[4] (iD) Martin Mikulics,[1] Claus M. Schneider,[1,5] (iD) and Roman Sobolewski[2,3] (iD)

AFFILIATIONS

[1] Research Centre Jülich, Peter Grünberg Institute, 52425 Jülich, Germany
[2] Materials Science Graduate Program and Laboratory for Laser Energetics, University of Rochester, Rochester, New York 14627-1299, USA
[3] Department of Electrical and Computer Engineering and Laboratory for Laser Energetics, University of Rochester, Rochester, New York 14627-0231, USA
[4] Research Centre Jülich, Ernst Ruska Centre for Microscopy and Spectroscopy with Electrons, 52425 Jülich, Germany
[5] Department of Physics, University of California Davis, Davis, California 95616-5270, USA

[a] Author to whom correspondence should be addressed: r.adam@fz-juelich.de

ABSTRACT

We generate terahertz (THz) transients by illuminating a few-nanometer-thick Ta/NiFe/Pt nanolayers with a train of linearly polarized 100-fs-wide laser pulses. The transients are $\sim$1-ps-wide free-space propagating bursts of electromagnetic radiations with amplitudes that are magnetically and optically tunable. Their spectral frequency content extends up to 5 THz, and the 3-dB cutoff is at 0.85 THz. The observed transient electromagnetic signals originate from the NiFe/Pt bilayer, and their amplitude dependence on the external magnetic field, applied in the sample plane, very closely follows the static magnetization versus magnetic field dependence of the NiFe film. For the same laser power, excitation with highly energetic, blue light generates THz transients with amplitudes approximately three times larger than the ones resulting from excitation by infrared light. In both cases, the transients exhibit the same spectral characteristics and are linearly polarized in the perpendicular direction to the sample magnetization. The polarization direction can be tuned by rotation of the magnetic field around the laser light propagation axis. The characteristics of our THz spintronic emitter signals confirm that THz transient generation is due to the inverse spin Hall effect in the Pt layer and demonstrate that ferromagnet/metal nanolayers excited by femtosecond laser pulses can serve as efficient sources of magnetically and optically tunable, polarized transient THz radiation.

Published under license by AIP Publishing. https://doi.org/10.1063/1.5099201

Terahertz (THz) radiation covers the electromagnetic spectrum range between radio-frequency millimeter waves and optical far-infrared radiation, approximately between 0.3 and 30 THz, and has been applied in astronomy, medical imaging, security, communication, and manufacturing,[1,2] as well as a scientific tool in materials testing[3] and bio imaging,[4] or in the study of electron wake-field acceleration.[5] Among different THz sources, currently, extensive research focuses on emitters of ultrafast electromagnetic transients with a broad THz-range spectrum, in order to control and capture spin,[6] charge,[7] or phase-transition related processes on subpicosecond time scales. Recent observation of THz emissions from optically excited ferromagnet/metal (F/M) nanolayers[8–13] establishes a very

elegant link between laser optics, spintronics, and THz radiation, merging these three very active scientific fields and having a tremendous potential for future applications. The uncomplicated fabrication of spintronic THz emitters can lead to widespread applications.

Superdiffusive spin currents generated in laser-driven demagnetization experiments have been theoretically predicted[14,15] and, subsequently, quickly confirmed in a number of experiments,[16–19] demonstrating their crucial role in ultrafast magnetization dynamics in a range of magnetic materials and structures. The central role of the superdiffusive currents in THz generation[9] has further strengthened their importance in the laser-driven spin transient dynamics and has led to applications that are currently emerging at the border of laser

physics and spin-based electronics. Two separate physical mechanisms have been proposed to explain the generation of THz transients from femtosecond laser-driven F/M bilayers and multilayers. In the first case, THz emission is explained by the photon-driven spin current flowing from an F film to a neighboring M material. This spin current is, subsequently, converted by the inverse spin Hall effect (ISHE) into a transient charge current flowing along the M surface, thereby generating a laser-helicity *independent* subpicosecond electromagnetic signal.[10,20] The other approach is based on breaking space-inversion symmetry resulting in the spin-galvanic effect at the F/M interface. This mechanism has been proposed to be responsible for the laser-helicity *dependent* transient THz generation and has been shown to vary strongly with the thickness of an interlayer X in Co/X/Pt trilayers.[21]

We have generated bursts of strong THz radiation (transient, single-picosecond electromagnetic signals) by placing Ta/NiFe/Pt (equivalently, Ta/Py/Pt, where Py stands for permalloy: $Ni_{80}Fe_{20}$) trilayers in a static magnetic field and illuminating it with a train of 100-fs-wide laser pulses from a commercial Ti:sapphire laser (800-nm wavelength and 76-MHz repetition rate). The train of laser pulses was split into two beams with a 90:10 intensity ratio. The high-intensity branch, after bouncing from a retroreflector mounted at the delay stage, was focused at our F/M sample using a concave optical lens with 50-mm focal length, while the low-intensity beam was used to excite a photo-conductive low-temperature grown GaAs (LT-GaAs) switch acting as a THz transient detector.[22] The linear motion of the delay stage in the probe beam, with a 2.5-μm-step size, allowed an optical path control with a 16.6-fs time resolution. Ta/Py/Pt samples were optically excited either by illumination of the metallic surface (direct geometry), or by laser pulses passing through the MgO substrate (reverse geometry). In addition, we used a Teflon (polytetrafluoroethylene) lens with a 5-mm diameter and 10-mm focal length to focus the THz radiation at the LT-GaAs detector operated in a photoconductive-sampling mode. The latter allowed us to reconstruct the THz transient in the time domain. The external **H** field was generated either by electromagnet coils wrapped around iron yokes and supplying a variable field of up to 70 kA/m, or by a pair of permanent magnets, generating a fixed, ~40 kA/m field.

Our spintronic samples consisted of Ta(2 nm)/Py(2 nm)/Pt(2 nm) nanotrilayers and were deposited sequentially at room temperature by magnetron sputtering on top of optically polished 10×10 mm^2 MgO substrates with (100) surface orientation. The deposition thickness for each layer was monitored by a quartz crystal microbalance. The thin, 2-nm Ta buffer layer was deposited first, directly on the MgO substrate in order to achieve a good adhesion and smoothness of the consecutive layers. We have chosen Pt as a top material for its relatively high spin–orbit coupling, the material-dependent parameter that, according to the literature, is responsible for THz generation in magnetic nano-layers.[23] We verified the latter by individually testing Py/Pt and Py/Ta nanobilayers, fabricated in a process analogous to the one described above.

Figure 1(a) presents a typical time-domain, subpicosecond (0.9-ps FWHM of the main peak) electromagnetic transient generated by our spintronic nanolayer emitter and detected by the LT-GaAs detector. The zero time on the time axis was chosen arbitrarily, but it was kept the same for all measurements. The measurement was done in the reverse geometry, illustrated in the left inset in Fig. 1(a) with the **H** field fixed at 55 kA/m and applied in the sample plane. The laser fluence was 7.25 μJ/cm^2. In this geometry, we have also observed (not shown here) a secondary, significantly weaker THz transient, delayed by ~10 ps with respect to the main signal. The latter signal was identified as a THz transient generated at the Py/Pt bilayer and propagating in the opposite direction with respect to the main one and, subsequently, reflected at the MgO/air interface. A fast Fourier transform (FFT) of the time-domain waveform is shown in the right inset in Fig. 1(a) as the normalized THz transient power spectrum. We note that the signal frequency content extends up to 5 THz with a 3-dB cutoff at 0.85 THz. A small dip visible in the power spectrum at about 2 THz corresponds to resonant absorption of a Teflon lens used to focus the THz beam. When we flipped the trilayer by 180° and illuminated it in the direct geometry, keeping the laser beam and **H** orientation unchanged, we recorded essentially the same time-domain transient as shown in the main panel of Fig. 1(a), but with the polarity reversed. As we discuss below, the latter indicates a reversed direction of the charge
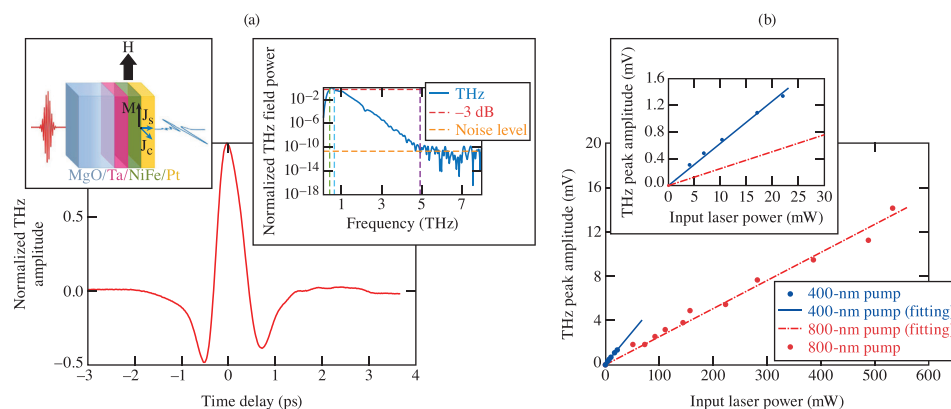
FIG. 1. (a) A normalized THz transient generated by a 100-fs-wide laser pulse impinging at a Ta/Py/Pt nanotrilayer through the MgO substrate (reverse illumination geometry). The top-left inset shows the trilayer stacking and the schematics of the THz-generation mechanism. The top-right inset presents a normalized THz power spectrum that corresponds to the pulse shown in the main panel. The spectrum exhibits a 3-dB cutoff at 0.85 THz and extends to 5 THz with exponentially decreasing intensity. (b) THz transient amplitude as a function of the incident laser beam power for both fundamental ($\lambda = 800$ nm; red solid circles) and frequency-doubled light ($\lambda = 400$ nm; blue solid circles). The inset shows the available power range for the 400 nm light and demonstrates a strongly increased efficiency of THz generation at the 400-nm wavelength.

current density $\mathbf{J_C}$. Compared to the reverse geometry, the signal in direct geometry had a slightly lower amplitude (apparently caused by THz absorption by Ta and MgO) and no secondary, reflected signal was observed. Finally, we optically illuminated the Pt/Py/Ta trilayer from the Pt side at a 45° incidence angle and collected a THz transient with the detector positioned at 90° with respect to the laser beam. As expected for superdiffusive current flowing in all directions, the recorded time-domain waveform had a shape identical to the pulse shown in the main panel of Fig. 1(a). The power spectra for the direct, reverse, and 45° illumination geometries were identical to that presented in Fig. 1(a), right inset. These measurements indicate that optically triggered THz transients originate near or at the Py/Pt interface. This observation was corroborated by our subsequent studies of Py/Ta and Py/Pt bilayers. Finally, we note that while the THz spectra obtained by us extend up to 5 THz, Seifert et al.[23] have reported significantly more broadband, up to 30 THz, transients generated from F/M nanolayers. In their studies, however, they used 10-fs-wide laser excitation pulses. Taking into account the fact that the duration of the spin current and the resulting charge current pulses should scale directly with the duration of the incident optical excitation, our 100-fs-wide pulses triggered approximately one order of magnitude longer electromagnetic bursts and, therefore, exhibited a tenfold lower frequency cutoff.

We have also studied the impact of varying external optical excitation on the THz signal emitted by our spintronic Ta/Py/Pt emitter. Figure 1(b) shows the maximum THz-signal amplitude A^{THz} dependence on the incident, average laser power at both the fundamental ($\lambda = 800$ nm; red solid circles) and frequency-doubled ($\lambda = 400$ nm; blue solid circles) wavelengths at a constant magnetic field $H = 55$ kA/m. In both cases, the dependence is linear, as indicated by the corresponding linear fits. Although the range of available incident powers for the 400-nm light was quite small, limited by the efficiency of the frequency-doubling barium borate (BBO) crystal, our data clearly demonstrate that for the same laser power, 400-nm photons generate approximately 3× larger subpicosecond transients, as compared to 800-nm ones. At the same time, the corresponding normalized time-domain waveforms (not shown) were practically the same as the one shown in Fig. 1(a), main panel, resulting in the identical THz power spectra. Although our data in Fig. 1(b) seem to contradict recent results by Herapath et al.,[24] where no wavelength dependence on THz generation was reported, we stress that the measurements in Ref. 24 were performed not only on a different material system, but, first of all, exclusively at infrared wavelengths (900–1500 nm). High-energy, blue photons used in our studies are certainly more efficiently absorbed by metallic nanolayers and generate larger (up to a factor of three, according to our measurements) concentration of hot electrons that give rise to an enhanced spin current. As a result, we observe the THz amplitude enhancement as it was discussed above and presented in Fig. 1(b).

In Fig. 2, we present the A^{THz} dependence on the magnitude of the in-plane **H** field applied to a Ta/Py/Pt nanolayer. An external electromagnet in our THz setup allowed us to tune the **H** field in a range up to ±70 kA/m. For a constant laser light ($\lambda = 800$ nm) with an average laser power of 550 mW, we stepped **H** from −70 kA/m to +70 kA/m and back to −70 kA/m, and for every **H** field value, we recorded an A^{THz} value. The experiment was performed in both the direct and reverse illumination geometries, and the corresponding results in the form of $A^{THz}(\mathbf{H})$ dependences are presented in Fig. 2 as
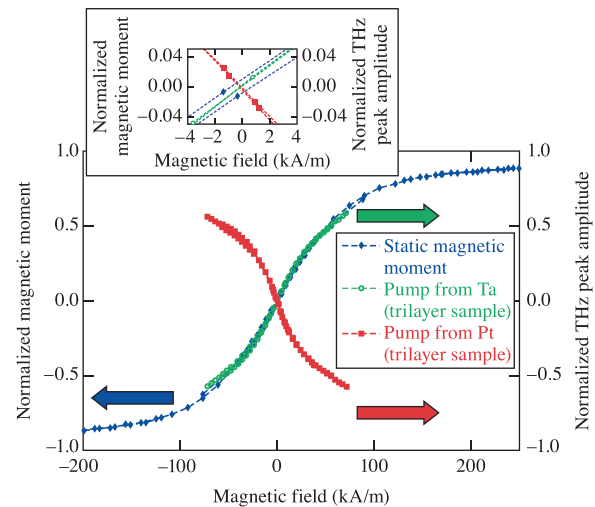

FIG. 2. Magnetic moment $\mu(\mathbf{H})$ (blue circles) and THz transient amplitudes $A^{THz}(\mathbf{H})$ of the Ta/Py/Pt trilayer for direct (red circles) and reverse (green circles) illumination geometries as a function of an external static magnetic field. To allow for a direct comparison, the $\mu(\mathbf{H})$ and $A^{THz}(\mathbf{H})$ curves were normalized at 60 kA/m. Contrary to the sample $\mu(\mathbf{H})$ dependence, the THz signal displays essentially no hysteresis (see inset). The dashed lines in the inset are simple data interpolations.

red and green circles, respectively. The additional blue circles in Fig. 2 correspond to the static hysteresis of the magnetic moment $\mu(\mathbf{H})$ of the Py nanolayer, recorded using a commercial physical property measurement system (PPMS). The $\mu(\mathbf{H})$ hysteresis loop shows that the 2-nm-thick Py film exhibits a coercive field H_C as low as 0.8 kA/m and reaches near-saturation at H above 160 kA/m. For direct comparison purposes, in Fig. 2, we normalized the PPMS and THz dependences at the $H = 60$ kA/m value. We note first that the $A^{THz}(\mathbf{H})$ hysteresis (green circles; reverse illumination) overlays perfectly the static $\mu(\mathbf{H})$ hysteresis measured using PPMS. When the sample is flipped into the direct geometry and the Pt film faces the laser light, the $A^{THz}(\mathbf{H})$ dependence is also inverted (red circles in Fig. 2) because of the reversed direction of $\mathbf{J_C}$, as already discussed in the context of the transient shown in Fig. 1(a). The red circles follow within the experimental error the inverted $\mu(\mathbf{H})$ dependence (not shown in the figure for clarity). The inset in Fig. 2 shows all three **H**-field dependences significantly expanded near the axis origin, and the dashed lines represent interpolations between experimental data points (color coding in the inset is the same as in the main panel). It points to a very interesting observation that the measured $A^{THz}(\mathbf{H})$ curves exhibit hysteresis significantly narrower than that of $\mu(\mathbf{H})$.

To confirm that the THz transient emission occurs solely at the Py/Pt interface, we additionally fabricated and tested two individual nanobilayers, namely, Py/Pt and Py/Ta, both on MgO substrates. As we expected on the basis of the results presented in Fig. 1, we could easily register THz emissions when we optically excited the Py/Pt sample. The $A^{THz}(\mathbf{H})$ dependences (not shown) for the direct and reverse geometries mimicked both qualitatively and quantitatively the ones presented in Fig. 2 for a Ta/Py/Pt nanotrilayer. On the other hand, within our experimental conditions (laser power and **H**), we did not see any signal generated by a Py/Ta nanobilayer.

At this point, it is reasonable to ask why $A^{\text{THz}}(\mathbf{H})$ for our samples follows the shape of the $\mu(\mathbf{H})$ hysteresis of the Py film constituting the F layer in both Ta/Py/Pt and Py/Pt samples. Our optical beam is linearly polarized, so we are in the laser-helicity *independent* case and the THz transient is directly proportional to $\mathbf{J_C}$ produced by the ISHE mechanism that in turn depends on the spin current density $\mathbf{J_S}$ and spin polarization $\boldsymbol{\sigma}$. According to, e.g., Ref. 25, $\mathbf{J_C} = D_{\text{ISHE}} (\mathbf{J_S} \times \boldsymbol{\sigma})$, where D_{ISHE} is a coefficient representing the ISHE efficiency in a material. Therefore, we can control the ultrafast time-domain signal amplitude and polarity by controlling the $\mathbf{J_C}$ amplitude and its direction. The $\mathbf{J_C}$ amplitude is controlled in our case through $\boldsymbol{\sigma} \sim \mu(\mathbf{H})$, while the $\mathbf{J_C}$ direction is controlled by the illumination geometry (direct or reverse). We note that in both geometries the superdiffusive current flows in all directions as confirmed by the experiment with laser illumination under 45° mentioned above; nevertheless, only the $\mathbf{J_C}$ component pointing from Py to Pt matters for THz generation. For fixed directions of $\mathbf{H}$ and $\mathbf{J_S}$, and because $\mathbf{J_C} \sim \mu(\mathbf{H})$, one should expect that $A^{\text{THz}}(\mathbf{H})$ shows the behavior similar/identical to the $\mu(\mathbf{H})$ dependence, as, indeed, is observed in our studies. The observed significantly narrower width of the $A^{\text{THz}}(\mathbf{H})$ hysteresis in the Ta/Py/Pt trilayer as compared to the $\mu(\mathbf{H})$ hysteretic dependence may arise from the fact that the static $\mu(\mathbf{H})$, measured in PPMS, represents a signal averaged over the whole sample volume. Therefore, for instance, pinning at the sample edges may contribute to signal, while THz generation is local, defined by a laser beam spot ($\sim 50 \, \mu m$ in diameter). Finally, we note that in order to generate THz transients in our soft magnetic Py-based samples with vanishing remanence, an external $\mathbf{H}$ field was always necessary. On the other hand, our preliminary measurements performed on magnetically harder materials show that after the initial magnetization, no external $\mathbf{H}$ is required to generate high-intensity THz transients. (Studies of transient THz emission from magnetically harder nanobilayers will be published separately.)

Finally, we have also measured the $A^{\text{THz}}(\mathbf{H})$ dependence on the angle φ of a constant $\mathbf{H}$ applied along the sample plane. An inset in Fig. 3 presents schematics of our experimental setup. In this case, our sample was mounted between two permanent magnets with their north and south poles aligned along the sample plane and the entire
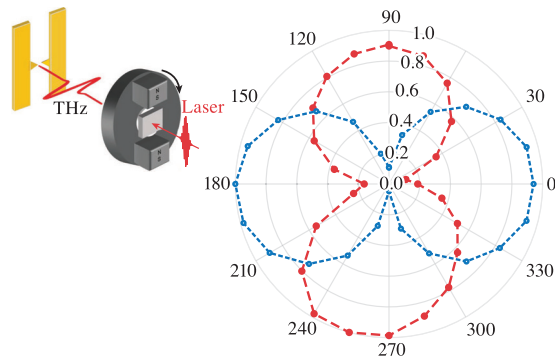
arrangement was attached to a rotating stage with a rotation accuracy of approximately 2°. The observed $A^{\text{THz}}(\varphi)$ dependence, presented in Fig. 3, main panel, is a result of the polarization-sensitive detection of the LT-GaAs detector and demonstrates that our THz transients are linearly polarized. The direction of maximum sensitivity is aligned along the triangular notches patterned in the coplanar waveguide of the detector (see the inset in Fig. 3), and the zero angle in Fig. 3 is defined as a horizontal alignment of the $\mathbf{H}$ field with respect to the laboratory frame. By rotating the sample and magnet assembly, we observe in Fig. 3 (red circles and a red dashed line) that the polarization of the emitted THz transient rotates, following the $\mathbf{H}$ alignment with an offset of 90° (e.g., horizontal THz polarization for the vertical magnetic field). Thus, for a fixed detector position, only the fraction of the THz-field intensity projected in the direction of the triangular notches is detected. The latter interpretation has been clearly confirmed by rotating the detector by 90° (not shown in Fig. 3 inset). The resulting THz intensity pattern is now rotated by 90° (blue circles and a blue dashed line Fig. 3). In future practical applications, THz polarization rotation can be easily transformed into amplitude tuning by placing a THz polarizer immediately after the spintronic emitter.

In conclusion, we have generated subpicosecond electromagnetic transients from Ta(2 nm)/Py(2 nm)/Pt(2 nm) spintronic nanotrilayers using a train of 100-fs-wide laser pulses with a fluence of up to 7.25 $\mu J/cm^2$ and a static magnetic field (up to $\pm 70 \, A/m$) applied in the plane of a sample. The resulting power spectra of the transients extend up to 5 THz with a 3-dB cutoff at 0.85 THz. The amplitude of the transients depends linearly on the average laser power. However, for the same laser power, blue photons (400-nm wavelength) generate THz transients with amplitudes approximately 3 times larger than transients resulting from excitation by infrared (800-nm-wavelength) photons. This shows that both the light intensity and the photon energy control $\mathbf{J_S}$, however with additionally increased efficiency at short excitation wavelengths. Our experiments conclusively show that in our Ta/Py/Pt emitters, transient THz signals are generated exclusively within the Py/Pt bilayer. The THz amplitude is tunable by the $\mathbf{H}$-field intensity and follows very closely the hysteretic behavior of the magnetization vs $\mathbf{H}$-field dependence of the Py layer, albeit $A^{\text{THz}}(\mathbf{H})$ is, in practice, nonhysteretic. Since the THz generation is linearly related to the amplitude of the induced $\mathbf{J_C}$, the THz amplitude can be tuned by controlling $\boldsymbol{\sigma}$ and $\mathbf{J_S}$, the quantities directly affecting $\mathbf{J_C}$. THz transients emitted by our spintronic emitter are linearly polarized. The direction of THz polarization is perpendicular to both the sample magnetization and the optically triggered superdiffusive spin current and can be controlled by rotating the $\mathbf{H}$-field direction around the sample surface normal. Finally, we note that our simple, robust, and tunable THz emitters can lead to widespread applications in compact, hand-held THz diagnostic devices, in local device-to-device communication with enormous data transfer capacity, or as sources for material and circuit testing at THz frequencies.

FIG. 3. Detected normalized THz intensity versus angle of the sample/magnet assembly $A^{\text{THz}}(\varphi)$ for the horizontal (red circles, dashed line) and vertical (blue circles, dashed line) detector orientations. $\varphi = 0$ refers to the horizontal alignment of magnetic field with respect to the laboratory frame. The inset shows schematics of the measurement setup for the horizontal detector orientation of the highest polarization sensitivity (vertical orientation not shown).

REFERENCES

[1]M. Tonouchi, Nat. Photonics **1**, 97 (2007); E. A. Williams, *National Association of Broadcasters Engineering Handbook*, 10th ed. (Elsevier, Burlington, MA, 2007).

[2]R. A. Lewis, J. Phys. D: Appl. Phys. **47**, 374001 (2014).

[3]A. Koroliov, G. Chen, K. M. Goodfellow, A. N. Vamivakas, Z. Staniszewski, P. Sobolewski, M. E. Fray, A. Łaszcz, A. Czerwinski, C. P. Richter, and R. Sobolewski, Appl. Sci. **9**, 391 (2019).

[4]K. Ajito and Y. Ueno, IEEE Trans. Terahertz Sci. Technol. **1**, 293 (2011).

[5]E. A. Nanni, W. R. Huang, K.-H. Hong, K. Ravi, A. Fallahi, G. Moriena, R. J. D. Miller, and F. X. Kärtner, Nat. Commun. **6**, 8486 (2015).

[6]S. Baierl, M. Hohenleutner, T. Kampfrath, A. K. Zvezdin, A. V. Kimel, R. Huber, and R. V. Mikhaylovskiy, Nat. Photonics **10**, 715 (2016).

[7]R. L. Milot, R. J. Sutton, G. E. Eperon, A. A. Haghighirad, J. M. Hardigree, L. Miranda, H. J. Snaith, M. B. Johnston, and L. M. Herz, Nano Lett. **16**, 7001 (2016).

[8]G. Torosyan, S. Keller, L. Scheuer, R. Beigang, and E. Th. Papaioannou, Sci. Rep. **8**, 1311 (2018).

[9]T. Seifert, S. Jaiswal, M. Sajadi, G. Jakob, S. Winnerl, M. Wolf, M. Kläui, and T. Kampfrath, Appl. Phys. Lett. **110**, 252402 (2017).

[10]T. Kampfrath, M. Battiato, P. Maldonado, G. Eilers, J. Nötzold, S. Mährlein, V. Zbarsky, F. Freimuth, Y. Mokrousov, S. Blügel, M. Wolf, I. Radu, P. M. Oppeneer, and M. Münzenberg, Nat. Nanotechnol. **8**, 256 (2013).

[11]Y. Wu, M. Elyasi, X. Qiu, M. Chen, Y. Liu, L. Ke, and H. Yang, Adv. Mater. **29**, 1603031 (2017).

[12]S.-Y. Xu, M. Neupane, C. Liu, D. Zhang, A. Richardella, L. A. Wray, N. Alidoust, M. Leandersson, T. Balasubramanian, J. Sánchez-Barriga, O. Rader, G. Landolt, B. Slomski, J. H. Dil, J. Osterwalder, T.-R. Chang, H.-T. Jeng, H. Lin, A. Bansil, N. Samarth, and M. Z. Hasan, Nat. Phys. **8**, 616 (2012).

[13]J. Walowski and M. Münzenberg, J. Appl. Phys. **120**, 140901 (2016).

[14]M. Battiato, K. Carva, and P. M. Oppeneer, Phys. Rev. Lett. **105**, 027203 (2010).

[15]M. Battiato, K. Carva, and P. M. Oppeneer, Phys. Rev. B **86**, 024404 (2012).

[16]D. Rudolf, C. La-O-Vorakiat, M. Battiato, R. Adam, J. M. Shaw, E. Turgut, P. Maldonado, S. Mathias, P. Grychtol, H. T. Nembach, T. J. Silva, M. Aeschlimann, H. C. Kapteyn, M. M. Murnane, C. M. Schneider, and P. M. Oppeneer, Nat. Commun. **3**, 1037 (2012).

[17]E. Turgut, C. La-o-vorakiat, J. M. Shaw, P. Grychtol, H. T. Nembach, D. Rudolf, R. Adam, M. Aeschlimann, C. M. Schneider, T. J. Silva, M. M. Murnane, H. C. Kapteyn, and S. Mathias, Phys. Rev. Lett. **110**, 197201 (2013).

[18]S. Mathias, C. La-O-Vorakiat, P. Grychtol, P. Granitzka, E. Turgut, J. M. Shaw, R. Adam, H. T. Nembach, M. E. Siemens, S. Eich, C. M. Schneider, T. J. Silva, M. Aeschlimann, M. M. Murnane, and H. C. Kapteyn, Proc. Natl. Acad. Sci. U.S.A. **109**, 4792 (2012).

[19]A. Eschenlohr, M. Battiato, P. Maldonado, N. Pontius, T. Kachel, K. Holldack, R. Mitzner, A. Föhlisch, P. M. Oppeneer, and C. Stamm, Nat. Mater. **12**, 332 (2013).

[20]J. Sinova, S. O. Valenzuela, J. Wunderlich, C. H. Back, and T. Jungwirth, Rev. Mod. Phys. **87**, 1213 (2015).

[21]G. Li, R. Mikhaylovskiy, K. A. Grishunin, J. D. Costa, Th. Rasing, and A. V. Kimel, J. Phys. D: Appl. Phys. **51**, 134001 (2018).

[22]A. Geižutis, A. Krotkus, K. Bertulis, G. Molis, R. Adomavičius, A. Urbanowicz, S. Balakauskas, and S. Valaika, Opt. Mater. **30**, 786 (2008).

[23]T. Seifert, S. Jaiswal, U. Martens, J. Hannegan, L. Braun, P. Maldonado, F. Freimuth, A. Kronenberg, J. Henrizi, I. Radu, E. Beaurepaire, Y. Mokrousov, P. M. Oppeneer, M. Jourdan, G. Jakob, D. Turchinovich, L. M. Hayden, M. Wolf, M. Münzenberg, M. Kläui, and T. Kampfrath, Nat. Photonics **10**, 483 (2016).

[24]R. I. Herapath, S. M. Hornett, T. S. Seifert, G. Jakob, M. Kläui, J. Bertolotti, T. Kampfrath, and E. Hendry, Appl. Phys. Lett. **114**, 041107 (2019).

[25]E. Saitoh, M. Ueda, H. Miyajima, and G. Tatara, Appl. Phys. Lett. **88**, 182509 (2006).